PNAS
www.pnas.org

Supplementary Information for

Inhibition of 3-phosphoinositide-dependent protein kinase 1 (PDK1) can revert cellular senescence in human dermal fibroblasts

Sugyun An[1,†], Si-Young Cho[2,†], Junsoo Kang[1], Soobeom Lee[1], Hyung-Su Kim[2], Dae-Jin Min[2], EuiDong Son[2] and Kwang-Hyun Cho[1*]

[1]Department of Bio and Brain Engineering, Korea Advanced Institute of Science and Technology (KAIST), Daejeon, Republic of Korea.

[2]AMOREPACIFIC Corp. R&D Unit, Gyeonggi-do, Republic of Korea

[†]S.A., and S.-Y.C. contributed equally to this study.

[*]Corresponding author. E-mail: ckh@kaist.ac.kr, Phone: +82-42-350-4325, Fax: +82-42-350-4310, Web: http://sbie.kaist.ac.kr/

This PDF file includes:

Figures S1 to S19
Tables S1 to S10
Legends for Dataset S1 to S2

Other supplementary materials for this manuscript include the followings:

Dataset S1 to S2

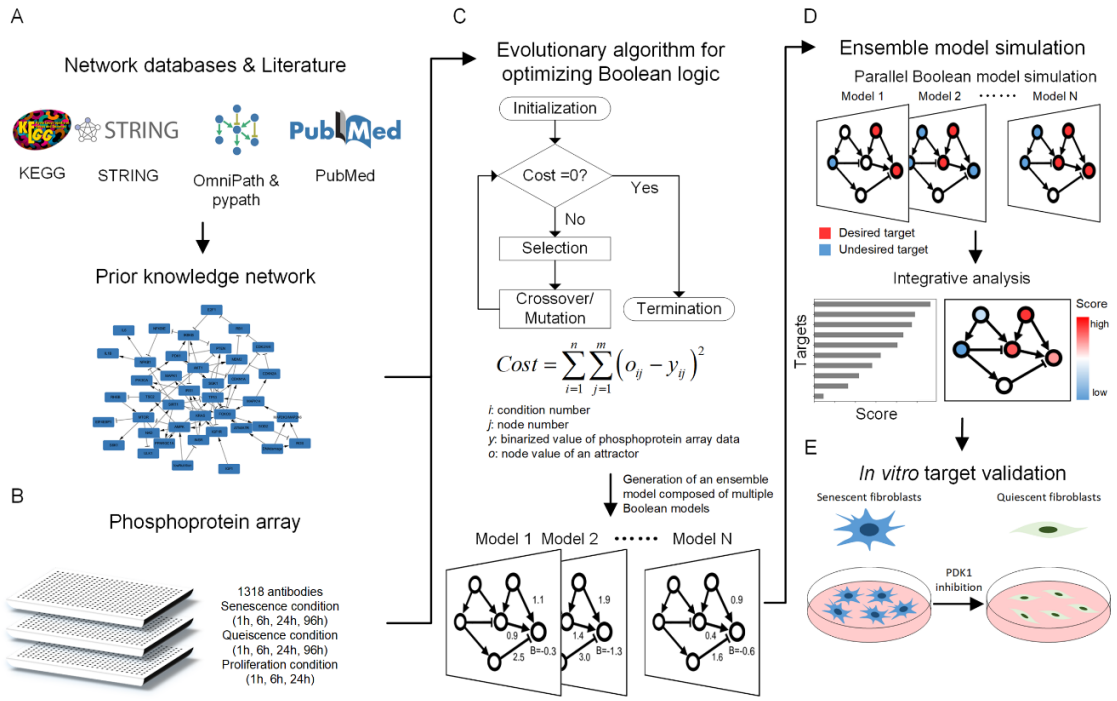

Fig. S1. Overview of network modeling, simulation, and validation. (A) Construction of a prior knowledge network. (B) Measurement of phosphoproteins in normal human dermal fibroblasts (NHDFs). Time-series phosphoprotein arrays were conducted for the senescence condition, quiescence condition, and proliferation condition. (C) Inference of Boolean logic of the cellular senescence network using an evolutionary algorithm. The cost function of the evolutionary algorithm is the sum of mean square error between protein states of binarized phosphoprotein array data and node states of attractors. Multiple Boolean network models that were optimized to the binarized phosphoprotein array data were generated and analyzed as an ensemble model. (D) Integrative analysis of the ensemble model for target identification. Inhibition simulations were conducted in each Boolean model and integrated into a score. (E) Experimental validation of senescence-to-quiescence inhibition target. The effect of PDK1 inhibition was measured in NHDFs.

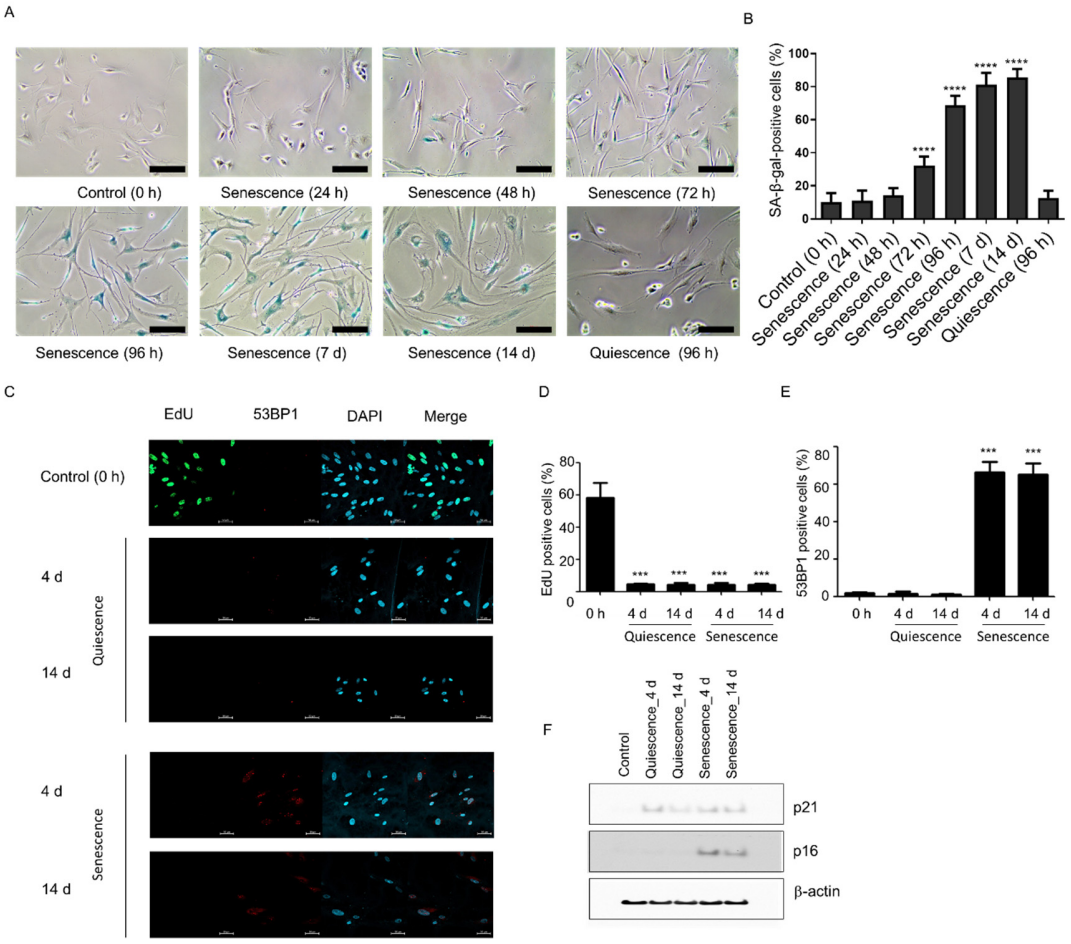

Fig. S2. Combination treatment of IGF-1 with doxorubicin effectively induces senescence in NHDFs. For induced senescence condition, NHDFs (PDL 12) were cultured in DMEM (4.5 g/L glucose) supplemented with 10% FBS, doxorubicin (100 ng/ml) and IGF-1 (100 ng/ml) for the indicated time. For induced quiescence condition, NHDFs (PDL 12) were cultured in DMEM (1 g/L glucose) supplemented with 1% FBS and doxorubicin (100 ng/ml) for the indicated time. NHDFs (PDL12) grown in DMEM (4.5 g/L glucose) media with 10% FBS were used as control. (A) Representative images of SA-β-gal staining activity. Scale bar= 500μm. (B) Bar diagram showing percentage of SA-β-gal positive cells. Mean ± SD (n=5), *** $P < 0.001$ compared to 0 h control senescent cells by one-way analysis of variance. (C) Representative immunofluorescent images of NHDFs stained for EdU (proliferating cells) and 53BP1 (cells with active DNA damage response). Scale bar = 50 μm. (D) Quantification of EdU as percentage of cells with positive staining. (E) Quantification of 53BP1-positive cells as percentage of cells with positive nuclear staining. For D and E, data are shown as mean ± SD (n=5), *** $P < 0.001$ compared with 0 h control cells by one-way analysis of variance. (F) Representative immunoblots showing the expression of p21 and p16. Data are representative of at least two independent experiments.

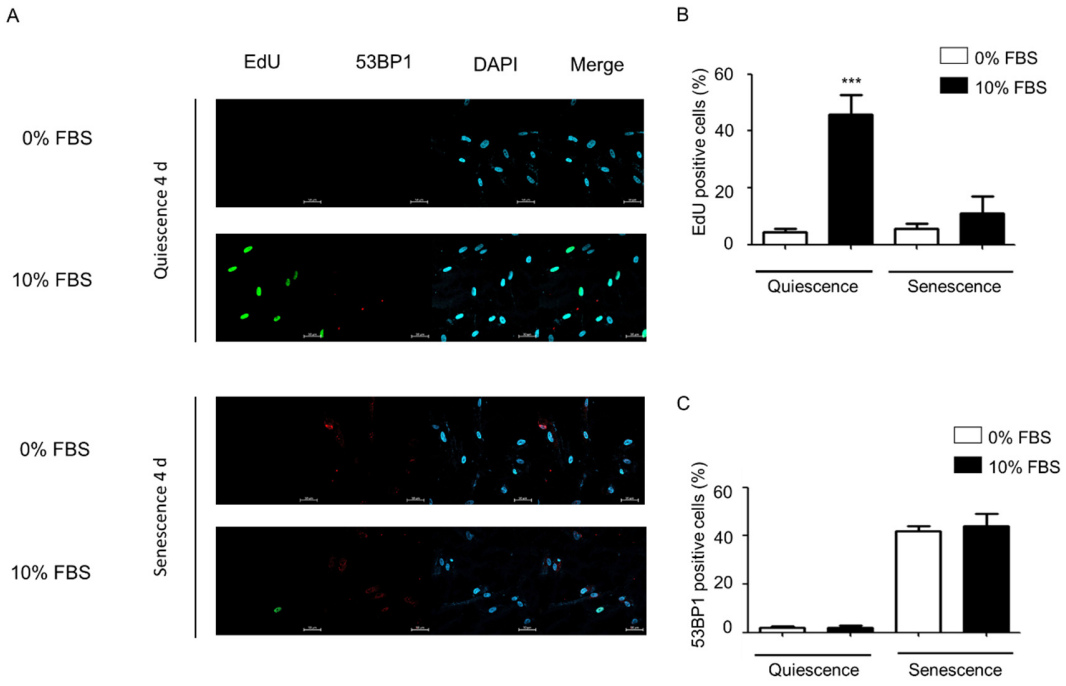

Fig. S3. The effects of doxorubicin alone or in combination with IGF-1 on senescence in NHDFs. For induced senescence condition, NHDFs (PDL 12) were cultured in DMEM (4.5 g/L glucose) supplemented with 10% FBS, doxorubicin (100 ng/ml) and IGF-1 (100 ng/ml) for 4 days. For induced quiescence condition, NHDFs (PDL 12) were cultured in DMEM (1 g/L glucose) supplemented with 1% FBS and doxorubicin (100 ng/ml) for 4 days. After 4 days, the NHDFs treated with doxorubicin alone or in combination with IGF-1 were incubated with 10 μM EdU in the presence or absence of 10% FBS for 16 h. (A) Representative immunofluorescent images of NHDFs stained for EdU (proliferating cells) and 53BP1 (cells with active DNA damage response). Scale bar = 50 μm. (B) Quantification of EdU as percentage of cells with positive nuclear staining. (C) Quantification of 53BP1-positive cells as percentage of cells with positive nuclear staining. For B and C, data are shown as mean ± SD (n=5), *** $P < 0.001$ compared cells without FBS by one-way analysis of variance.

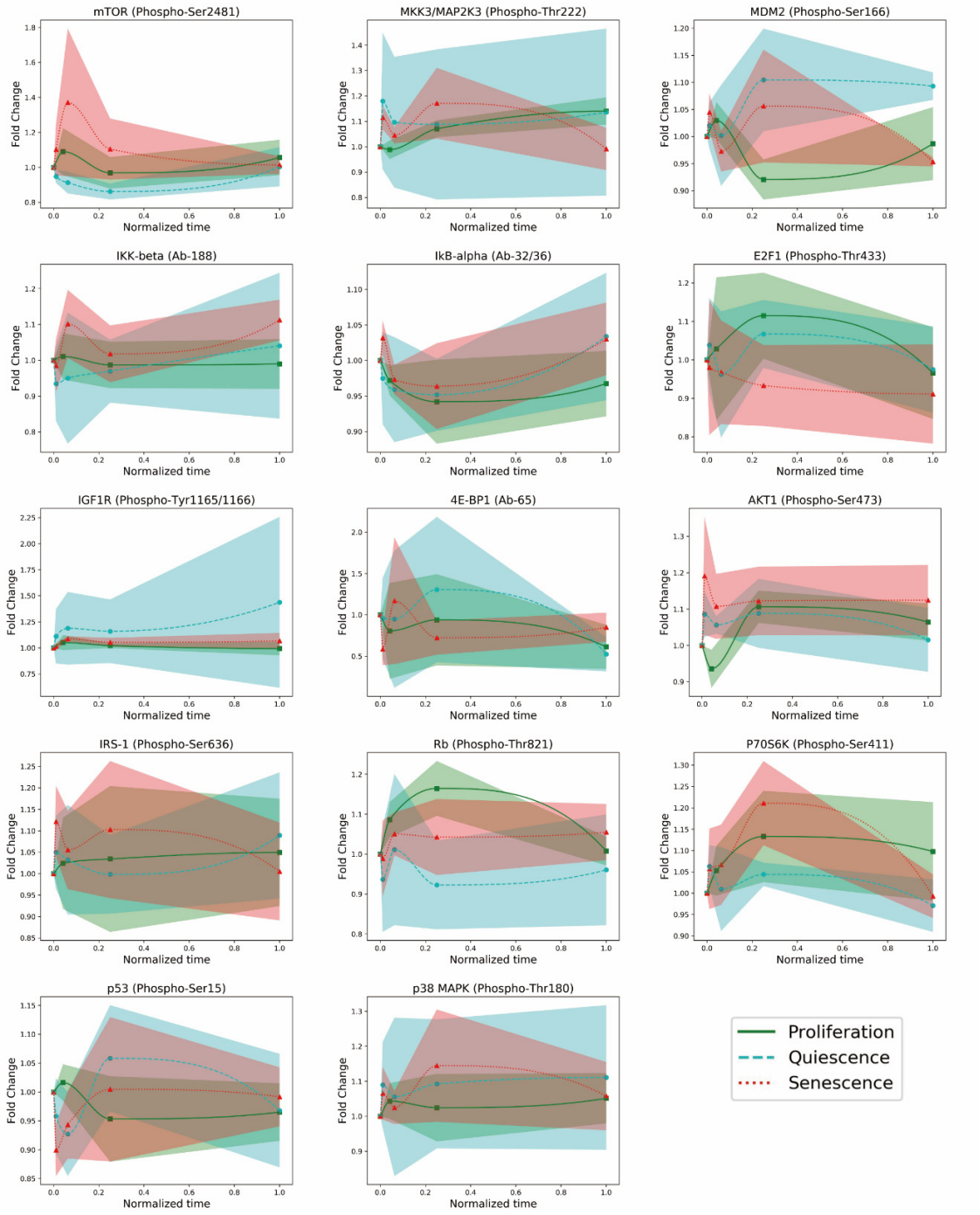

Fig. S4. The time course measurements of 14 key proteins obtained from phosphoprotein array. Fold changes along with normalized time under proliferation, quiescence and senescence conditions are plotted (see the Methods section). Points indicate mean fold change values. Shaded error bands show median absolute deviations (n=4).

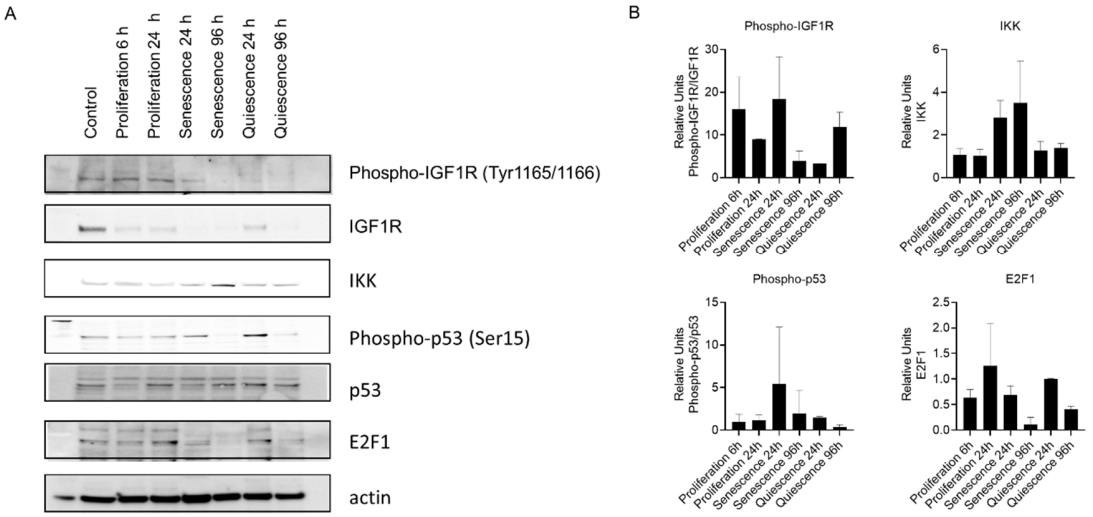

Fig. S5. Immunoblot analysis and quantification. (A) Immunoblot showing the abundance of the indicated proteins or phosphorylated proteins in NHDFs. For induced senescence condition, NHDFs (PDL 12) were cultured in DMEM (4.5 g/L glucose) supplemented with 10% FBS, doxorubicin (100 ng/ml) and IGF-1 (100 ng/ml) for the indicated times. For induced quiescence condition, NHDFs (PDL 12) were cultured in DMEM (1 g/L glucose) supplemented with 1% FBS and doxorubicin (100 ng/ml) for the indicated times. For proliferation, NHDFs were cultured in DMEM (4.5 g/L glucose) supplemented with 10% FBS and IGF-1 (100 ng/ml) for the indicated times. NHDFs (PDL12) grown in DMEM (1 g/L glucose) media with 1% FBS were used as control. Cell lysates were subjected to immunoblot analysis using antibodies against the indicated proteins. Data are representative of at least two independent experiments. (B) Immunoblot quantification. Data are shown as means ± SD (n = 2).

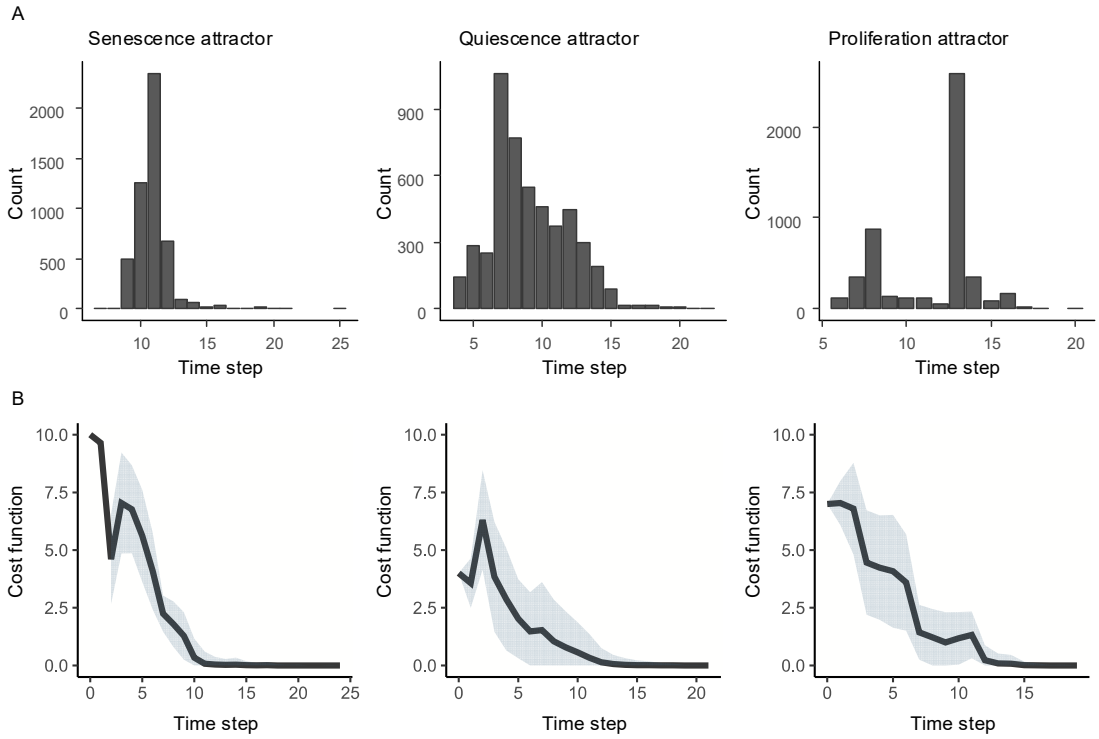

Fig. S6. Time steps and cost function values for the Boolean models reaching the senescence, quiescence, or proliferation attractors. (A) The bar graphs show the time steps taken for 5000 Boolean network models to reach their respective attractors. (B) The line graphs show the average value of the cost function for Boolean network models at each time step. Shaded error bands show standard deviations.

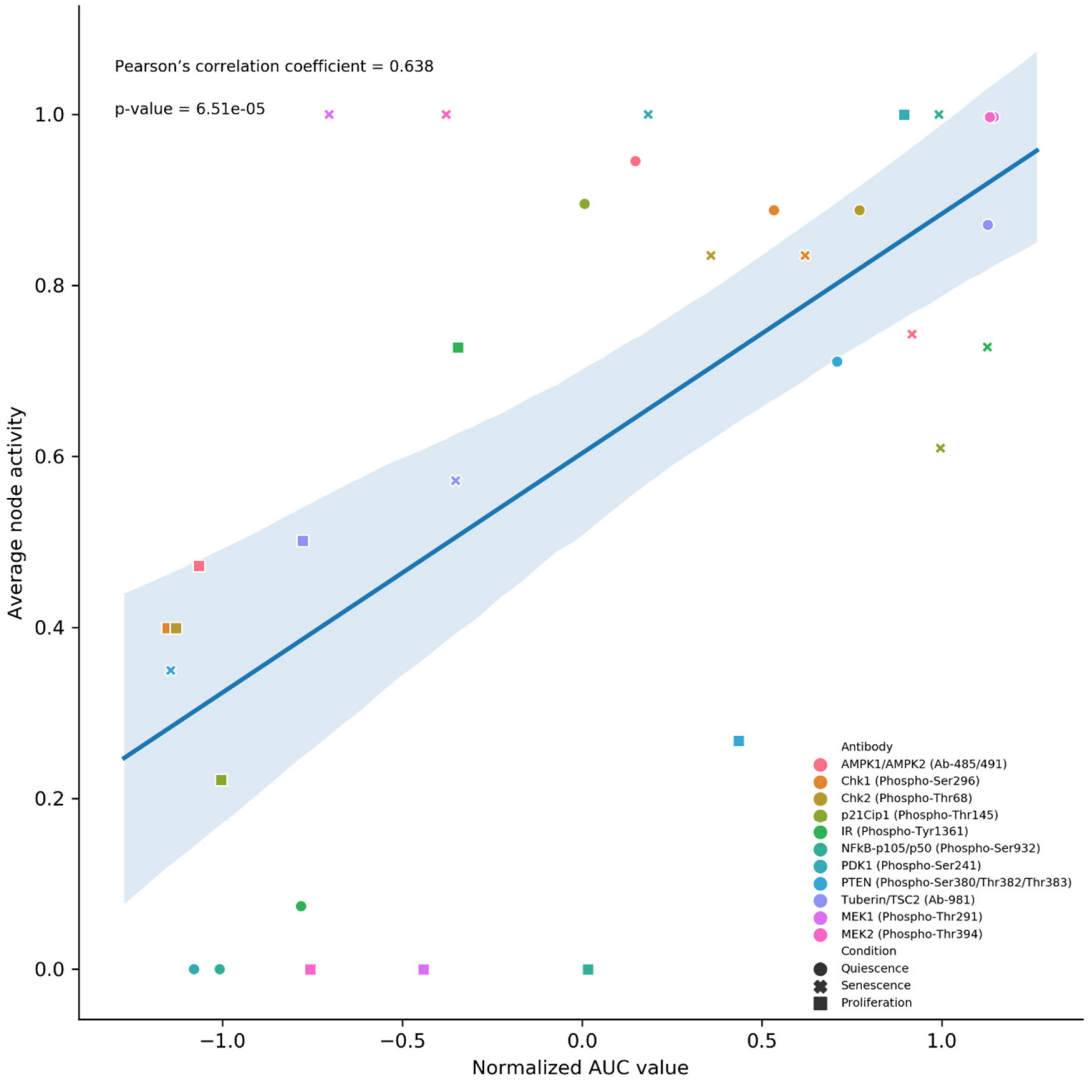

Fig. S7. Scatter plot and regression line of normalized AUC value on average node activity. Normalized AUC value (x-axis) is a representative value of time-series phosphoprotein array data (see Methods for details). Average node activity (y-axis) is the average value of node states (0 or 1) of 5000 Boolean network models after the models reached their respective attractors under each of conditions. See Table S6 for the corresponding node in the network model for each antibody. A blue line is the regression line and a translucent band around the line shows 95% confidence interval. The antibodies are marked with different colors. The conditions are marked with different shapes. Pearson's correlation and two-tailed p-value are shown in the upper left corner.

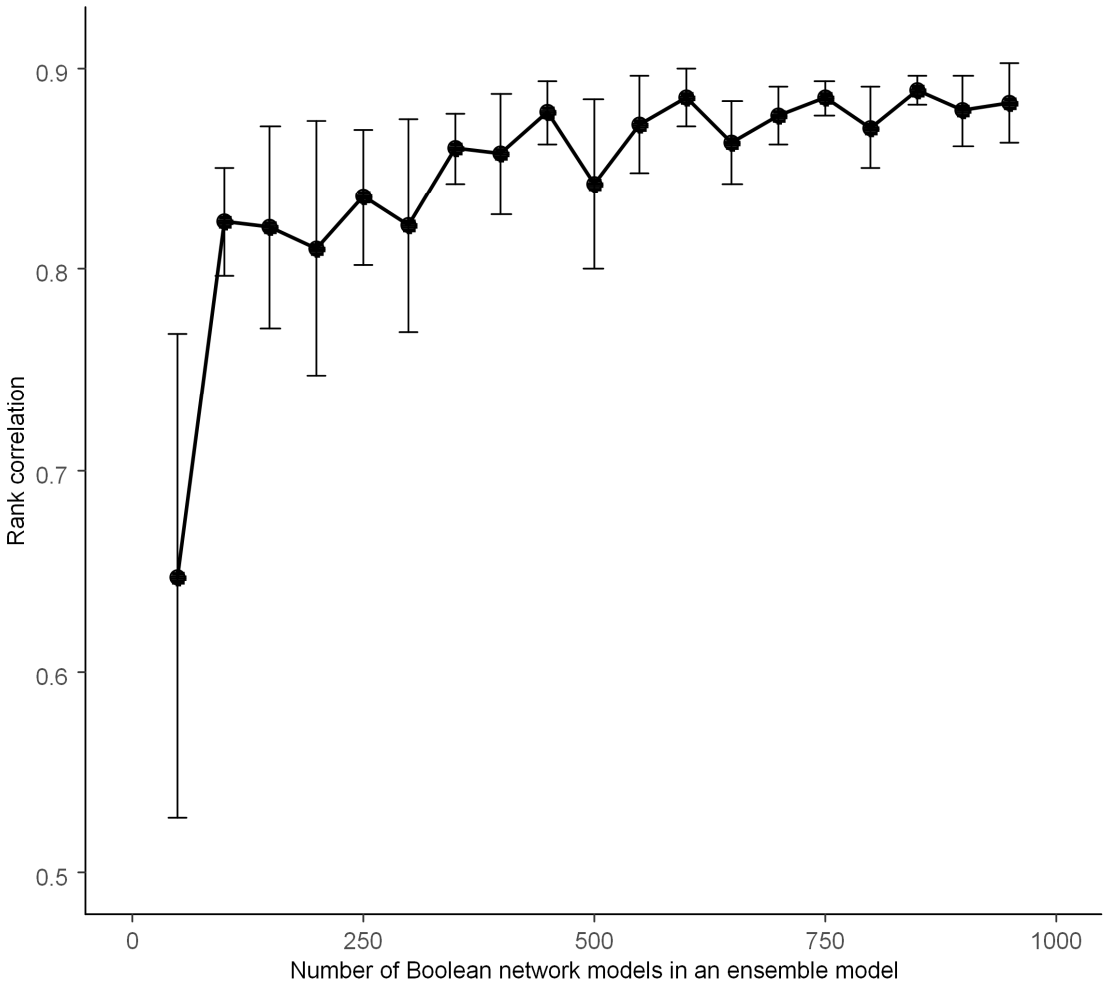

Fig. S8. Rank correlation of identified targets for senescence reversion by the number of Boolean network models in an ensemble model. We simulated pairs of ensemble models with a specific number of different Boolean network models to identify targets for senescence reversion, and we evaluated their Spearman rank-order correlation. The plot shows the Spearman rank-order correlation according to increasing number of Boolean network models in an ensemble model. The error bars represent standard deviations (n=10).

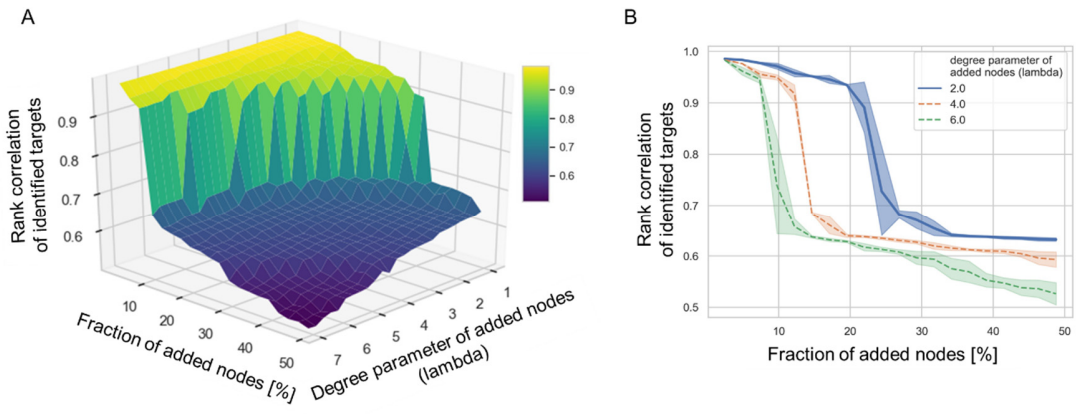

Fig. S9. Robustness analysis of the rank correlation of identified targets for senescence reversion with respect to network perturbations. We performed extensive simulations of the effects of senescence reversion by controlling the identified targets from perturbed networks, which are networks with randomly added nodes that represent kinases or regulators we possibly missed, and evaluated the resulting rank correlations. The added nodes were randomly connected to the nodes within the network excluding the input and output nodes. The number of connections (degree) that each of these added nodes are followed by the Poisson distribution with a specific lambda parameter. The targets of senescence reversion in rank from perturbed networks were compared to the results from the original network. For this comparison, weighted Kendall Tau rank correlation was used where rank r is mapped to weight $1/(r+1)^2$ in order to emphasize higher ranking targets. (A) 3D plot showing the robustness analysis results of rank correlations with respect to the fraction of added nodes and degree parameter. X-axis denotes the fraction of randomly added nodes against the total number of nodes in the network, y-axis denotes a lambda parameter of the Poisson distribution, and z-axis denotes weighted Kendall Tau rank correlation results of senescence reversion. (B) Average value of weighted Kendall Tau rank correlations for different values of lambda. Shaded error bands represent standard deviations (n=20). The solid blue line (lambda=2) shows the rank correlation results of senescence reversion with the degree distribution of added nodes closest to that of the original network.

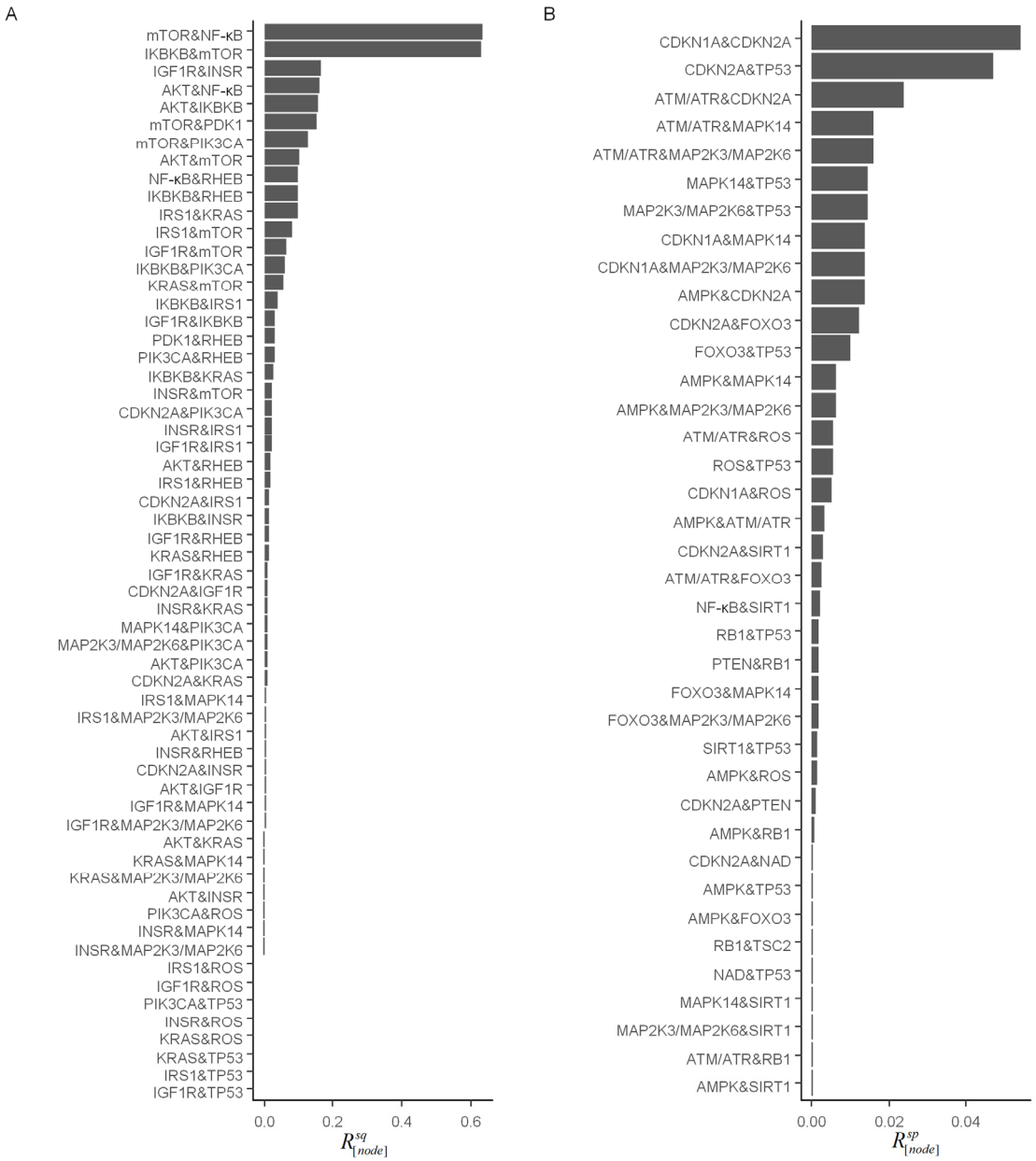

Fig. S10. Double node inhibition simulation results. (A) The bar graph shows the ratio of Boolean network models for which double node inhibition converts the senescence state into the quiescence state ($R^{sq}_{[node]}$). (B) The bar graph shows the ratio of Boolean network models for which double node inhibition converts the senescence state into the proliferation state ($R^{sp}_{[node]}$).

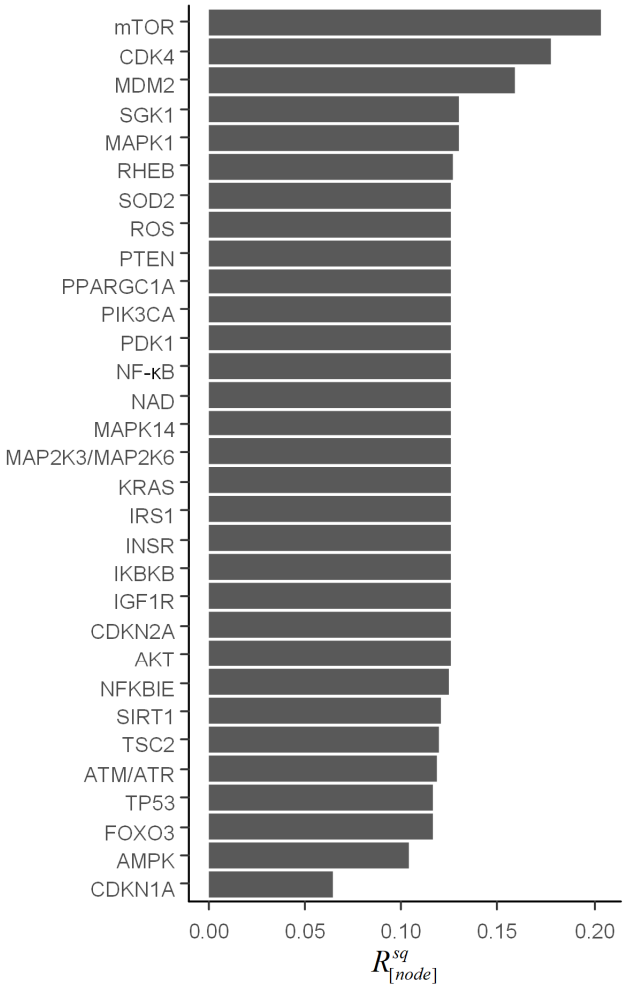

Fig. S11. Single node inhibition simulation results using an ensemble model with simplified Boolean models. Boolean models were simplified by converting network logical parameter values into 1, -1 or 0 according to the sign of their optimized parameter values. The bar graph shows the ratio of simplified Boolean network models for which the node inhibition converts the senescence state into the quiescence state ($R^{sq}_{[node]}$). There was no node for which its inhibition converted the senescence attractor to the proliferation attractor ($R^{sp}_{[node]}$) in an ensemble model with simplified Boolean models.

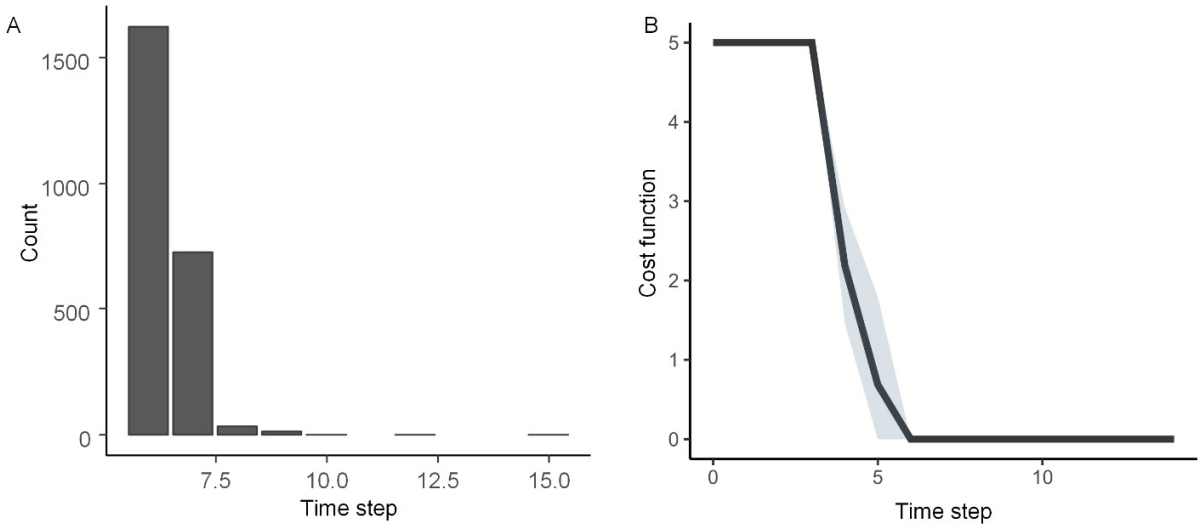

Fig. S12. Transition from senescence attractor to quiescence attractor by PDK1 inhibition. The 2401 Boolean network models in which PDK1 was detected as the senescence-reversing target were analyzed. (A) The bar graph shows counts of Boolean network models by time step took for Boolean network models to reach the quiescence attractor from senescence attractor by PDK1 inhibition. (B) Average value of cost function of Boolean network models at each time step. Shaded error bands show standard deviations (n=2401).

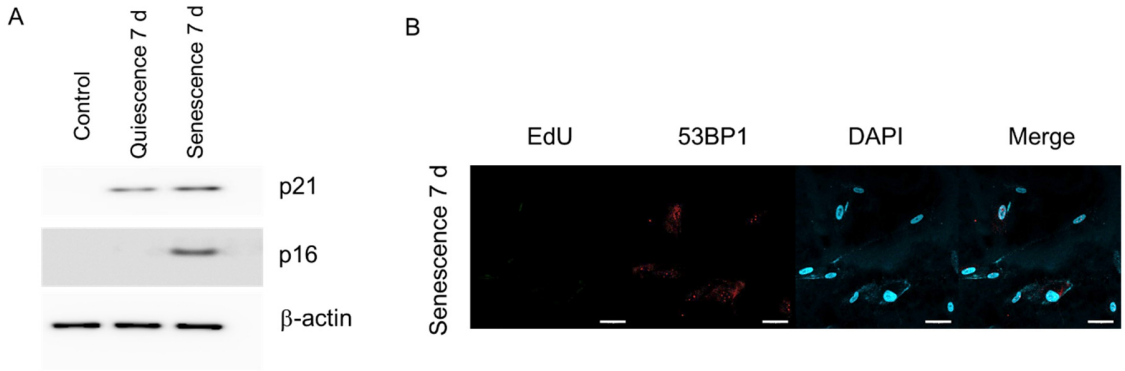

Fig. S13. Immunoblots and immunofluorescent images of NHDFs under senescence on day 7. For induced senescence condition, NHDFs (PDL 12) were cultured in DMEM (4.5 g/L glucose) supplemented with 10% FBS, doxorubicin (100 ng/ml) and IGF-1 (100 ng/ml) for 7 days. For induced quiescence condition, NHDFs (PDL 12) were cultured in DMEM (1 g/L glucose) supplemented with 1% FBS and doxorubicin (100 ng/ml) for 7 days. NHDFs (PDL12) grown in DMEM (4.5 g/L glucose) media with 10% FBS were used as control. (A) Representative immunoblot showing p16 and p21 expression levels. Data are representative of at least two independent experiments. (B) Representative immunofluorescent images of senescent NHDFs for 7 days stained for EdU (proliferating cells) and 53BP1 (cells with active DNA damage response). Scale bar = 50 μm.

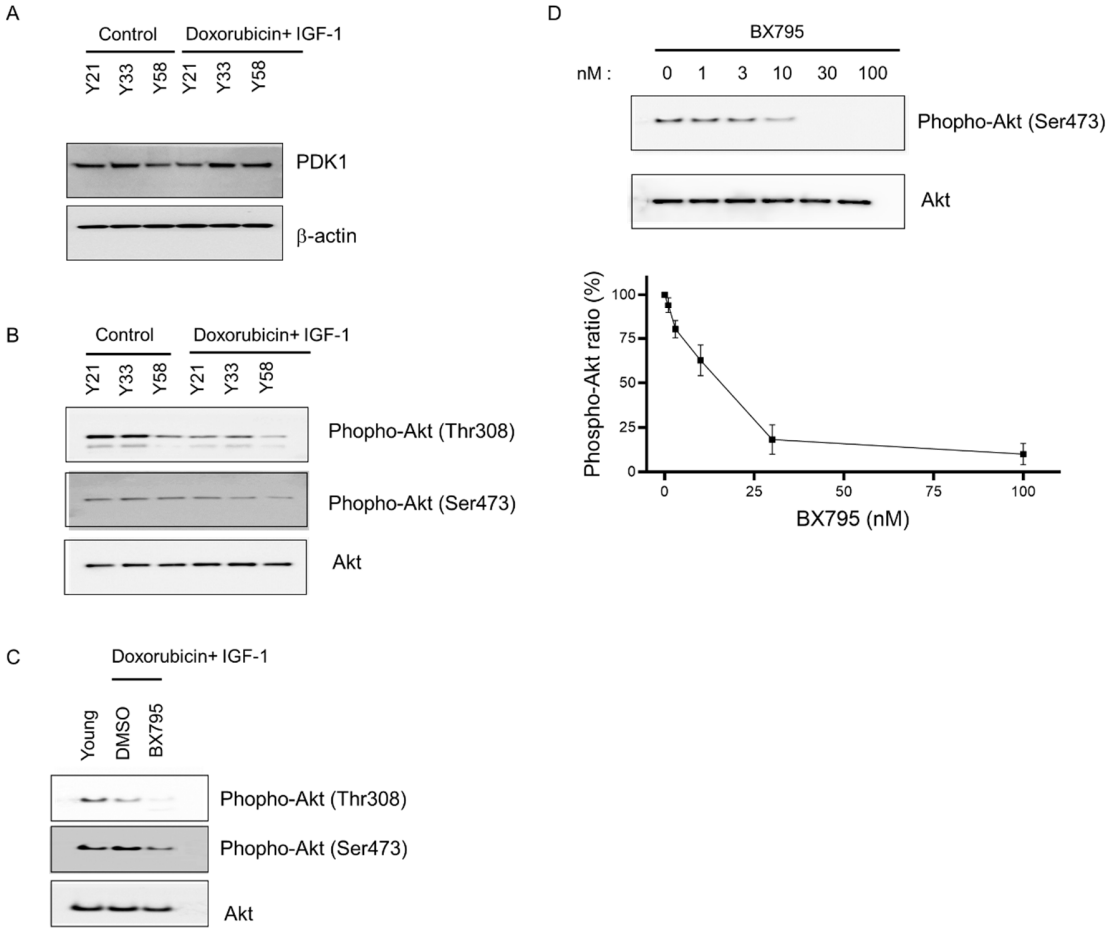

Fig. S14. PDK1 expression level and Akt phosphorylation level in NHDFs derived from different donors (a 21-year-old, a 33-year-old, and a 58-year-old females). For induced senescence condition, NHDFs from donors of indicated ages (PDL 12) were cultured in DMEM (4.5 g/L glucose) supplemented with 10% FBS, doxorubicin (100 ng/ml) and IGF-1 (100 ng/ml) for 7days. Representative immunoblots showing (A) PDK1 expression levels and (B) Akt phosphorylation levels in NHDFs from the skin of female donors of different ages (21, 33, and 58) upon senescence induction. Data are representative of at least two independent experiments. (C) Akt phosphorylation levels in Y33 NHDFs upon senescence induction in the presence or absence of PDK inhibition. NHDFs were induced to senescence by treatment with doxorubicin (100 ng/ml) plus IGF-1 (100 ng/ml) for 7 days. The senescent cells were then exposed to DMSO or BX795 (100 nM) for 7 more days and analyzed its effect on phospho-Akt (Thr308), phospho-Akt (Ser473), and total Akt levels by immunoblotting. Young NHDFs were not subjected to senescence condition or drug treatment. Data are representative of at least two independent experiments. (D) BX795 inhibits phosphorylation of Akt (Ser473) in Y33 NHDFs. Y33 NHDFs were treated with vehicle or various concentration of BX795 for 30 min. The phosphorylation of Akt (Ser473) was determined by immunoblotting as described in Methods. The graph represents the percentage of phosphorylation ratio (phosphorylated/total) compared to phosphorylation ratio without the inhibitor, BX795 (mean ± SEM, n=3).

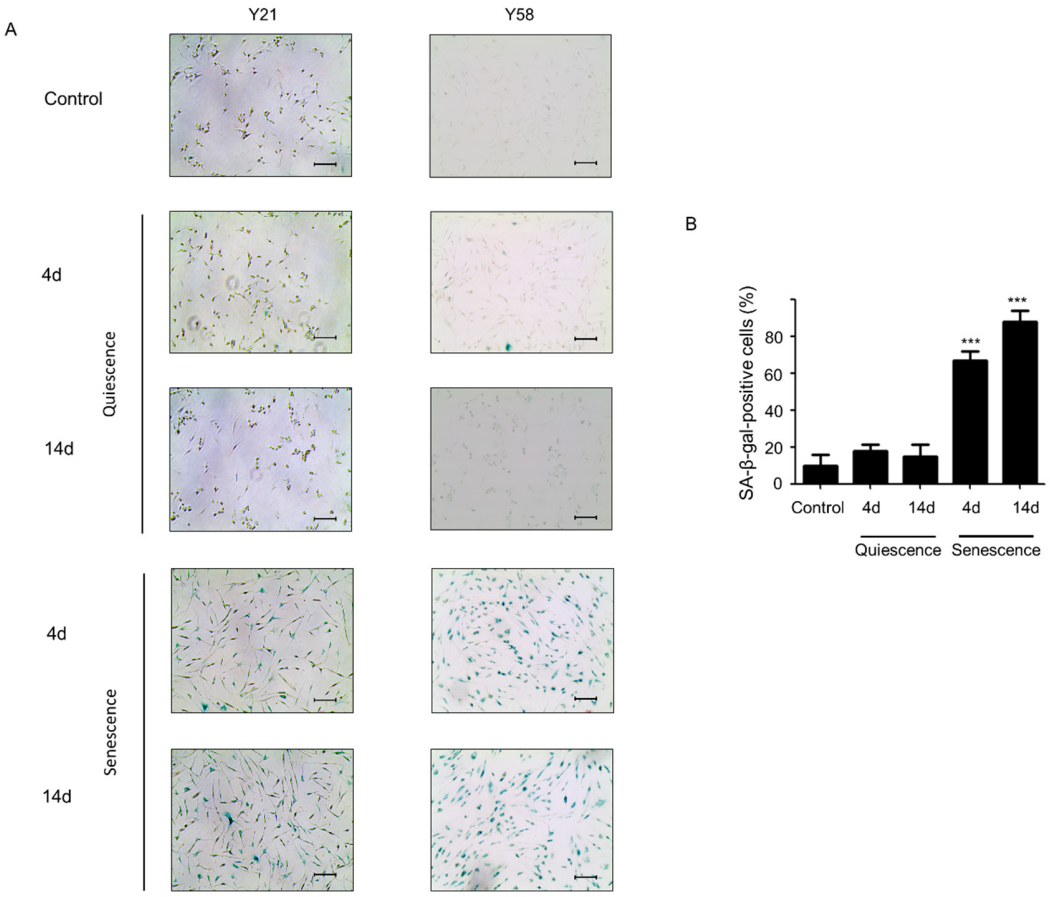

Fig. S15. Cell morphology and SA-β-gal activity in NHDFs derived from different donors (a 21-year-old and a 58-year-old females) during induction of senescence or quiescence. For induced senescence condition, NHDFs from donors of indicated ages (PDL 12) were cultured in DMEM (4.5 g/L glucose) supplemented with 10% FBS, doxorubicin (100 ng/ml) and IGF-1 (100 ng/ml) for the indicated time. For induced quiescent condition, NHDFs (PDL 12) were cultured in DMEM (1 g/L glucose) supplemented with 1% FBS and doxorubicin (100 ng/ml) for the indicated time. NHDFs (PDL12) grown in DMEM (4.5 g/L glucose) media with 10% FBS were used as control. (A) Representative images of SA-β-gal staining activity. Scale bar= 200μm. (B) Bar diagram showing SA-β-gal positive cells in percentage. Mean ± SD (n=5), *** $P < 0.001$ compared to control cells by one-way analysis of variance.

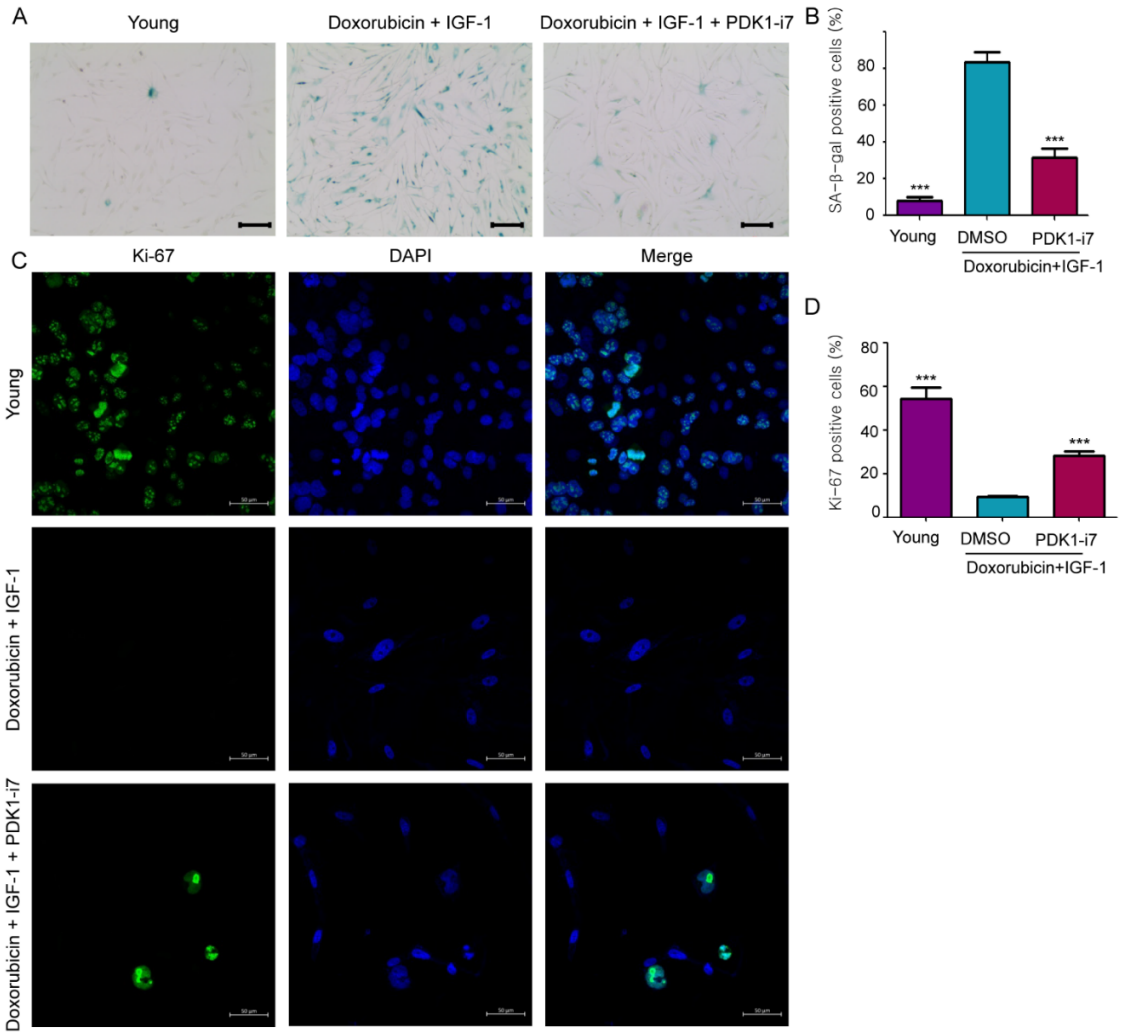

Fig. S16. Senescence-associated phenotypes following PDK1 inhibitor 7 in NHDFs. Young NHDFs were not subjected to senescence conditions or drug treatment. Young NHDFs were analyzed at PDL 12. NHDFs were induced to senescence by treatment with doxorubicin (100 ng/ml) plus IGF-1 (100 ng/ml) for 7 days. These cells were then treated with DMSO or PDK1-inhibitor 7 (PDK1-i7, 10 nM) for 7 more days. (A) Representative image of SA-β-gal staining. Scale bar = 200 μm. (B) Bar diagram showing percentage of SA-β-gal positive cells. (C) Representative immunofluorescent images of NHDFs stained for Ki-67. Scale bar = 50 μm. (D) Quantification of the percentages of Ki-67-positive cells. Mean ± SD (n=5), *** $P < 0.001$ compared to DMSO control senescent cells by one-way analysis of variance.

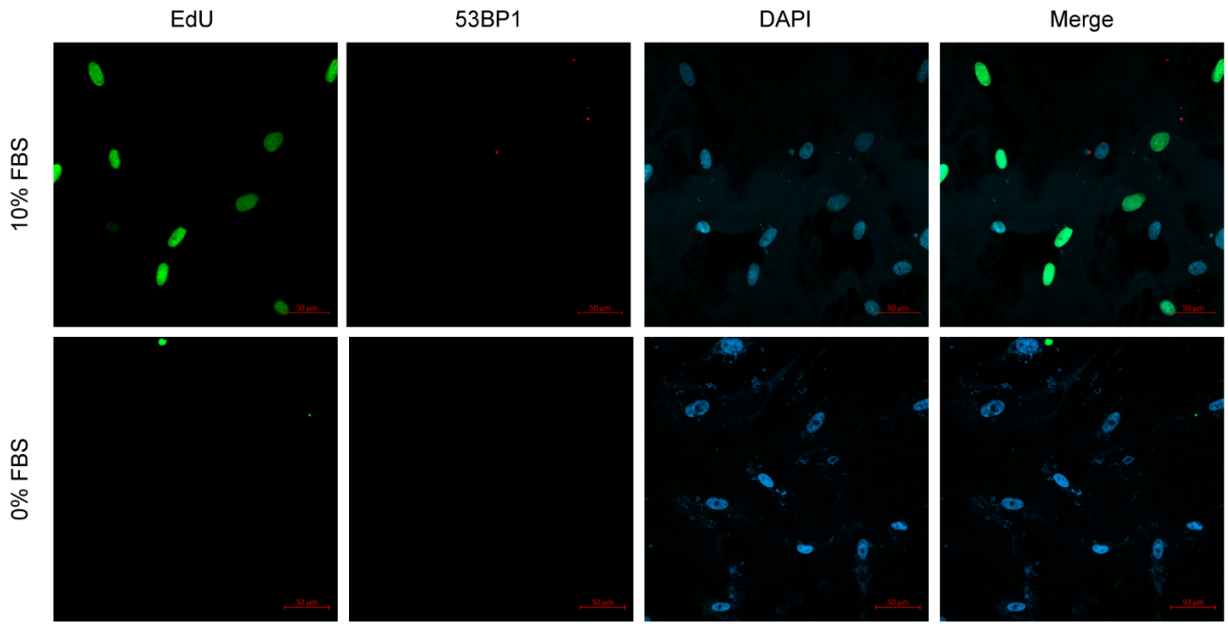

Fig. S17. Proliferation of reverted cells. NHDFs (PDL 12) were induced to senescence by treatment with doxorubicin (100 ng/ml) plus IGF-1 (100 ng/ml) for 7 days. The cells were then treated with BX795 (100 nM) in the presence of doxorubicin and IGF-1 for 7 more days. The BX795-treated cells were incubated with 10 μM EdU in the presence or absence of 10% FBS for 16 h. Representative immunofluorescent images of NHDFs stained for Edu, 53BP1, and DAPI. Scale bar = 50 μm.

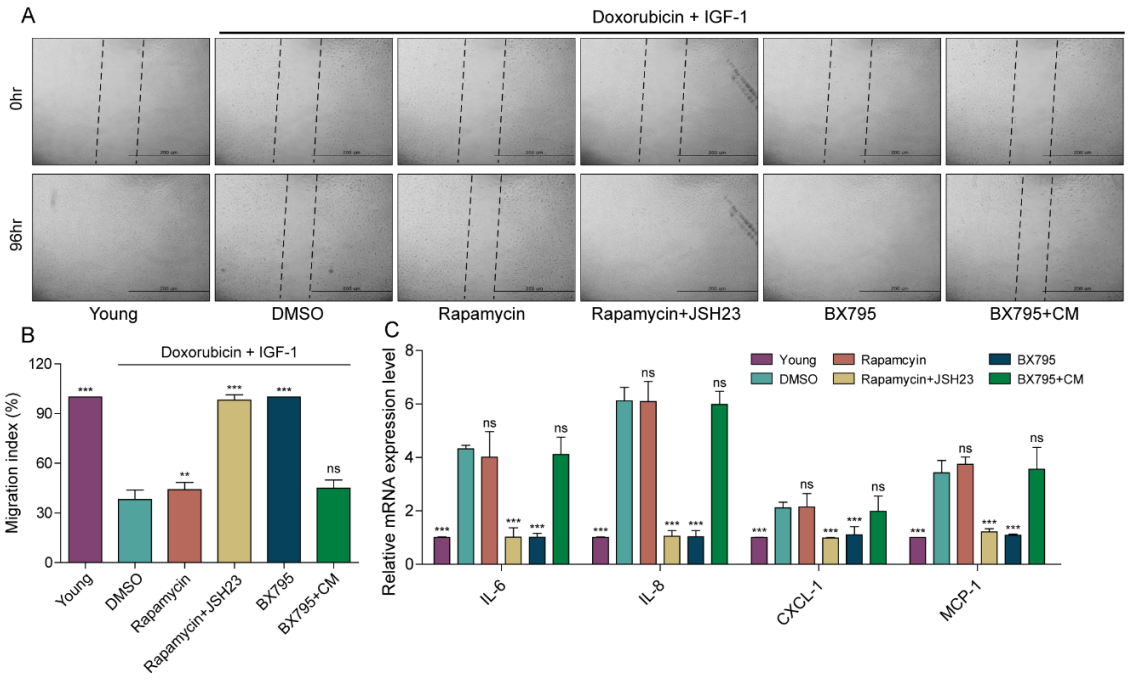

Fig. S18. Functional recovery from senescence by PDK1 inhibition analyzed by wound-healing assay. Young NHDFs were not subjected to senescence conditions or drug treatment. Young NHDFs were analyzed when cultures reached approximately 80% confluence at PDL 12. The remaining NHDFs were induced to senescence by 7-day exposure to doxorubicin (100 ng/ml) plus IGF-1 (100 ng/ml). For drug-treated conditions, the senescent cells were then treated with DMSO, rapamycin (100 nM), rapamycin plus JSH23 (2.5μM), or BX795 (100 nM) for 7 more days. For conditioned medium treatment (BX795 + CM), cells were grown in the presence of doxorubicin and IGF-1 for 7 days, followed by 7 days in the additional presence of doxorubicin, IGF-1, and BX795, were subcultered, and then were incubated with conditioned medium from senescent cells for 3 more days. (A) Representative images from 0 h and 96 h post-wounding are shown. Dashed lines mark the wound area. Scale bar = 200 μm. (B) Quantification analysis of migration area in scratch wound assay. Mean ± SD (n=3), *** $P < 0.001$ compared to DMSO control senescent cells by one-way analysis of variance. (C) mRNA expression levels of SASP genes measured with qRT-PCR analysis. Mean ± SD (n=5), ** $P < 0.01$ or *** $P < 0.001$ compared to DMSO control senescent cells by one-way analysis of variance.

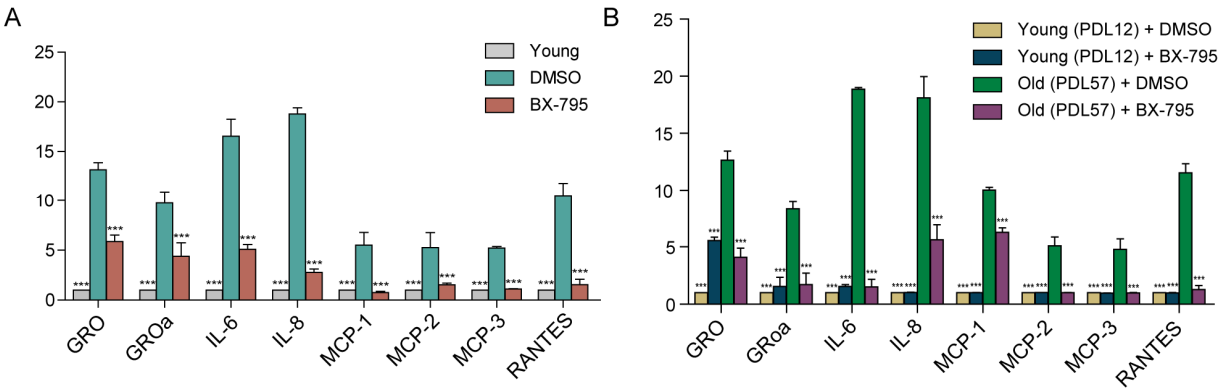

Fig. S19. PDK1 inhibition suppresses the SASP in skin equivalents. 3D skin models (skin equivalents) were prepared from young NHDFs (PDL 12) or senescent NHDFs induced into senescence by doxorubicin plus IGF-1 or repeated plating (replicative senescence, PDL 57) were exposed to DMSO or BX795. Conditioned medium (CM) from skin equivalents from chemical-induced or replicative senescent NHDFs treated with or without BX795 were measured with a cytokine antibody array and were normalized to internal positive controls on each membrane. (A) Secreted protein measured in a cytokine array of skin equivalents from chemical-induced NHDFs treated with or without BX795. (B) Secreted protein measured in a cytokine array of skin equivalents from replicative senescent NHDFs treated with or without BX795. Mean ± SD (n=3), ***P < 0.001 by compared to DMSO control senescent cells by one-way analysis of variance.

Table S1. The 41 nodes composing the cellular senescence network

Name	Gene symbol	Entrez ID	Uniprot ID
AKT	AKT1	207	P31749
AMPK	PRKAA1, PRKAA2, PRKAB1	5562, 5563,5564	Q13131, P54646,Q9Y478
ATM/ATR	ATM, ATR	472, 545	Q13315, Q13535
CDK4	CDK2, CDK4, CDK6	1017, 1019, 1021	P24941, P11802, Q00534
CDKN1A	CDKN1A	1026	P38936
CDKN2A	CDKN2A	1029	Q8N726
DNA damage	-	-	-
E2F1	E2F1	1869	Q01094
4E-BP1	EIF4EBP1	1978	Q13541
FOXO3	FOXO3	2309	O43524
IGF-1	IGF1	3479	P05019
IGF1R	IGF1R	3480	P08069
IKBKB	IKBKB	3551	O14920
IL-8	CXCL8	3576	P10145
IL-6	IL6	3569	P05231
INSR	INSR	3643	P06213
IRS1	IRS1	3667	P35568
KRAS	KRAS, HRAS	3845, 3265	P01116, P01112
MAP2K3/MAP2K6	MAP2K3, MAP2K6	5606, 5608	P46734, P52564
MAPK1	MAPK1	5594	P28482
MAPK14	MAPK14	1432	Q16539
MDM2	MDM2	4193	Q00987
mTOR	MTOR	2475	P42345
NAD	-	-	-
NF-κB	NFKB1	4790	P19838
NFKBIE	NFKBIA, NFKBIE	4792, 4794	P25963, O00221
PDK1	PDPK1	5170	O15530
PIK3CA	PIK3CA	5290	P42336
PPARGC1A	PPARGC1A	10891	Q9UBK2
PTEN	PTEN	5728	P60484
RB1	RB1	5925	P06400
RHEB	RHEB	6009	Q15382
ROS	-	-	-
S6K1	RPS6KB1	6198	P23443
SGK1	SGK1	6446	O00141
SIRT1	SIRT1	23411	Q96EB6
SOD2	SOD2	6648	P04179
TP53	TP53	7157	P04637
TSC2	TSC2	7249	P49815
ULK1	ULK1	8408	O75385
Low nutrition	-	-	-

Table S2. The 77 links composing the cellular senescence network

Source node	Regulation type	Target node	Mechanism	PMID	Database
AKT	-	CDKN1A	phosphorylation	11463845	Omnitpah;STRING
AKT	-	FOXO3	phosphorylation	12517744	Omnitpah;STRING
AKT	+	IKBKB	phosphorylation	11259436	Omnitpah;STRING
AKT	+	MDM2	phosphorylation	11923280	Omnitpah;STRING
AKT	+	mTOR	phosphorylation	16027121	Omnitpah;STRING
AKT	-	PTEN	ubiquitination	26183061	Omnitpah;STRING
AKT	-	TSC2	phosphorylation	12172553	Omnitpah;STRING
AMPK	+	FOXO3	phosphorylation	22186033	Omnitpah;STRING
AMPK	-	mTOR	phosphorylation	22186033	Omnitpah;STRING
AMPK	+	NAD	metabolism	19262508	KEGG;STRING
AMPK	+	PPARGC1A	transcription	23963743	Omnitpah;STRING
AMPK	+	TP53	phosphorylation	22186033	Omnitpah;STRING
AMPK	+	TSC2	phosphorylation	22186033	Omnitpah;STRING
AMPK	+	ULK1	phosphorylation	22186033	Omnitpah;STRING
ATM/ATR	+	TP53	phosphorylation	9925639	KEGG;Omnipath;STRING
CDK4	-	RB1	phosphorylation	24089445	KEGG;Omnipath;STRING
CDKN1A	-	CDK4	binding	24089445	KEGG;Omnipath;STRING
CDKN2A	-	CDK4	binding	24089445	KEGG;Omnipath;STRING
CDKN2A	-	MDM2	binding	9724636	KEGG;Omnipath;STRING
DNA damage	+	ATM/ATR	input		
DNA damage	+	MAP2K3/MAP2K6	input		
DNA damage	+	ROS	input		
FOXO3	+	ATM/ATR	phosphorylation	22893124	Omnitpah;STRING
FOXO3	+	CDKN1A	transcription	28808415	KEGG;STRING
FOXO3	+	SOD2	transcription	26184557	KEGG;STRING
IGF-1	+	IGF1R	input		
IGF1R	+	IRS1	phosphorylation	26474286	KEGG;Omnipath;STRING
IGF1R	+	KRAS	Indirect	23658296	STRING
IKBKB	-	IRS1	phosphorylation	22982470	KEGG;Omnipath;STRING
IKBKB	-	NFKBIE	phosphorylation	10602459	Omnitpah;STRING
IKBKB	-	PTEN	transcription	14729949	STRING
INSR	+	IRS1	binding	20966354	KEGG;Omnipath;STRING
INSR	+	KRAS	GTP-GDP conversion	20966354	Omnitpah;STRING
IRS1	+	PIK3CA	binding	20966354	KEGG;Omnipath;STRING
KRAS	+	MAPK1	phosphorylation	11942415	KEGG;STRING
KRAS	+	PIK3CA	binding	21779497	KEGG;Omnipath;STRING
Low nutrition	+	AMPK	input		
Low nutrition	-	INSR	input		
MAP2K3/MAP2K6	+	MAPK14	phosphorylation	11942415	KEGG;Omnipath;STRING
MAPK1	-	FOXO3	phosphorylation	18204439	Omnitpah;STRING
MAPK14	+	CDKN2A	transcription	19619499	KEGG;STRING
MAPK14	+	FOXO3	phosphorylation	22128155	Omnitpah;STRING
MAPK14	+	TP53	phosphorylation	17481747	KEGG;Omnipath;STRING
MDM2	-	FOXO3	ubiquitination	21238503	Omnitpah;STRING
MDM2	-	RB1	ubiquitination	15577944	KEGG;Omnipath;STRING
MDM2	-	TP53	ubiquitination	23885265	KEGG;Omnipath;STRING
mTOR	-	4E-BP1	phosphorylation	12080086	KEGG;Omnipath;STRING
mTOR	+	PPARGC1A	transcription	18046414	STRING
mTOR	+	S6K1	phosphorylation	12080086	KEGG;Omnipath;STRING
mTOR	-	ULK1	phosphorylation	21258367	KEGG;Omnipath;STRING
NAD	+	SIRT1	chemical reaction	22106091	KEGG
NF-κB	+	IL-8	transcription	22182507	KEGG;STRING
NF-κB	+	IL-6	transcription	22182507	KEGG;STRING
NF-κB	+	MAPK1	indirect	16644866	STRING
NFKBIE	-	NF-κB	binding	10602459	Omnitpah;STRING
PDK1	+	AKT	phosphorylation	25295225	Omnitpah;STRING
PDK1	+	IKBKB	indirect	15802604	
PDK1	+	SGK1	phosphorylation	28236975	KEGG;Omnipath;STRING
PIK3CA	+	PDK1	binding	25295225	KEGG;STRING
PTEN	-	PDK1	indirect	25295225	KEGG;STRING

RB1	-	E2F1	transcription	24089445	KEGG;Omnipath;STRING
RHEB	+	mTOR	binding	15854902	KEGG;Omnipath;STRING
ROS	+	MAP2K3/MAP2K6	indirect	20112989	
SGK1	-	FOXO3	phosphorylation	11154281	Omnitpah;STRING
SIRT1	+	FOXO3	deacetylation	14976264	KEGG;Omnipath;STRING
SIRT1	-	NF-κB	deacetylation	23029496	KEGG;STRING
SIRT1	+	PPARGC1A	deacetylation	21396404	KEGG;Omnipath;STRING
SIRT1	-	TP53	deacetylation	12220851	KEGG;Omnipath;STRING
SIRT1	+	TSC2	deacetylation	20169165	STRING
SOD2	-	ROS	chemical reaction	22302046	KEGG
TP53	+	CDKN1A	transcription	24089445	KEGG;Omnipath;STRING
TP53	-	IGF1R	indirect	29273484	STRING
TP53	+	MDM2	transcription	14707283	KEGG;Omnipath;STRING
TP53	+	PTEN	transcription	11545734	KEGG;Omnipath;STRING
TSC2	-	RHEB	binding	12842888	KEGG;Omnipath;STRING
E2F1	-	IKBKB	binding	27185527	
TP53	+	AMPK	indirect	27454290	STRING

Table S3. Experimental conditions of phosphoprotein array

		Quiescence	Senescence	Proliferation
Media condition	IGF-1	-	100ng/ml	100ng/ml
	FBS	1%	10%	10%
	Glucose	1g/ml	4.5g/ml	4.5g/ml
Doxorubicin		100ng/ml	100ng/ml	-
Time points		1h, 6h, 24h, 96h	1h, 6h, 24h, 96h	1h, 6h, 24h

Table S4. Summary of the phosphoprotein array data and supporting literatures for binarized AUC values of the 14 key proteins. From RPPA experiments (n=4), mean fold changes of 14 key proteins at each time point were used to calculate AUC values. These AUC values were z-score normalized and then binarized based on threshold values (see Threshold value column) inferred from previous studies (see PMID column). 11 out of 14 AUC values of key proteins were well in accord with the previous experimental observations reported in the literature. The AUC value of IGF1R under quiescence condition did not match the reports in the literature. However, our western blot results on IGF1R in Fig. S4. show that IGF1R level is lowest in quiescence condition, consistent with the previous findings. Given that IGF1R is a direct downstream target of IGF1, which is an input condition for both senescence and proliferation condition, we have concluded that the western blot results reflected IGF1R level better than the RPPA results. The AUC value of MDM2 under proliferation condition also did not match the reports in the literature. However, MDM2 is known to form a negative feedback loop with p53 (1, 2) which is inactivated under proliferation condition in both phosphoprotein array and western blot results in Fig. S4. Given ample citations on p53-MDM2 interaction, p53 phosphoprotein array and western blot results, we have decided the binarized AUC value of MDM2 under proliferation to 1, since the binarized AUC value of p53 under proliferation is 0. Lastly, the AUC value of NFKBIA under senescence condition did not match the reports in the literature. However, NFKBIA is directly inhibited by IKBKB (3) which is noticeably activated under senescence condition in both phosphoprotein array and western blot results in Fig. S4. Considering ample citations and our experimental results, we have decided the binarized AUC value of NFKBIA under senescence to 0, since the binarized AUC value of IKBKB under senescence is 1. We marked these three amended values in blue.

Gene symbol	Antibody	AUC			Normalized AUC			Binarized AUC			Threshold value	PMID
		Q	S	P	Q	S	P	Q	S	P		
EIF4EBP1	4E-BP1 (Ab-65)	1.10	0.80	0.86	1.39	-0.93	-0.45	1	0	0	0	21750861 30602778
AKT1	AKT1 (Phospho-Ser473)	1.07	1.12	1.075	-0.80	1.41	-0.61	0	1	1	-0.7	22481935 21909130
E2F1	E2F1 (Phospho-Thr433)	1.04	0.93	1.08	0.37	-1.37	1.00	0	0	1	0.5	11719808 16596252
IGF1R	IGF1R (Phospho-Tyr1165/1166)	1.23	1.06	1.01	1.38	-0.43	-0.95	0	1	1	-	28945762 28966916
NFKBIA	IkB-alpha (Ab-32/36)	0.97	0.98	0.95	0.33	1.02	-1.36	1	0	1	-	9738011 21979375
IKBKB	IKK-beta (Ab-188)	0.99	1.04	0.99	-0.65	1.41	-0.77	0	1	0	0	29292732 26946493
IRS1	IRS-1 (Phospho-Ser636)	1.02	1.08	1.04	-1.07	1.34	-0.27	0	1	1	-0.5	23478262 26474286
MAP2K3	MKK3/MAP2K3 (Phospho-Thr222)	1.10	1.12	1.09	-0.24	1.33	-1.09	1	1	0	-0.5	22404972 26573462
MTOR	mTOR (Phospho-Ser2481)	0.90	1.09	1.00	-1.25	1.19	0.06	0	1	1	0	19117990 31316753
MAPK14	p38 MAPK (Phospho-Thr180)	1.10	1.11	1.03	0.49	0.90	-1.39	1	1	0	0	22404972 26573462
TP53	p53 (Phospho-Ser15)	1.02	0.99	0.96	1.23	-0.01	-1.22	1	1	0	-0.5	9681831 23416979
RPS6KB1	P70S6K (Phospho-Ser411)	1.03	1.15	1.12	-1.37	0.99	0.38	0	1	1	0	25379019 10942600
RB1	Rb (Phospho-Thr821)	0.94	1.04	1.12	-1.27	0.10	1.17	0	0	1	0.5	26160835 29577907
MDM2	MDM2 (Phospho-Ser166)	1.09	1.03	0.95	1.17	0.10	-1.27	0	0	1	-	9681831 29402901

Table S5. Average node activities for each attractor

Condition / Node	Senescence	Quiescence	Proliferation	Senescence + PDK1 Inhibition
AKT	1	0	1	0
AMPK	0.743024	0.945439	0.472303	0.743024
ATM/ATR	0.835069	0.887963	0.399417	0.876302
CDK4	0.078717	0.046647	0.593503	0.047897
CDKN1A	0.609746	0.89546	0.221991	0.884215
CDKN2A	1	0.996876	0	0.997918
DNA damage	1	1	0	1
E2F1	0	0	1	0
4E-BP1	0	1	0	1
FOXO3	0.429404	0.796127	0.091628	0.723449
IGF-1	1	0	1	1
IGF1R	1	0	1	1
IKBKB	1	0	0	0
IL-8	1	0	0	0
IL-6	1	0	0	0
INSR	0.72803	0.073303	0.72803	0.72803
IRS1	1	0	1	1
KRAS	0.898376	0.349021	0.898376	0.898376
MAP2K3/MAP2K6	1	0.996876	0	0.997918
MAPK1	0.913369	0.60808	0.740941	0.740941
MAPK14	1	0.996876	0	0.997918
MDM2	0	0	1	0
mTOR	1	0	1	0
NAD	0.671387	0.729696	0.607247	0.671387
NF-κB	1	0	0	0
NFKBIE	0	1	1	1
PDK1	1	0	1	0
PIK3CA	0.999584	0.001249	0.999584	0.999584
PPARGC1A	0.931695	0.853811	0.905873	0.806747
PTEN	0.349854	0.710954	0.267389	0.710954
RB1	1	1	0	1
RHEB	0.322366	0.216576	0.342774	0.224073
ROS	0.612661	0.588297	0.232403	0.593919
S6K1	1	0	1	0
SGK1	0.76718	0.492711	0.76718	0.492711
SIRT1	0.618492	0.640983	0.613078	0.618492
SOD2	0.622657	0.722407	0.542274	0.70304
TP53	1	1	0	1
TSC2	0.571845	0.870887	0.501458	0.830487
ULK1	0	1	0	1
Low nutrition	0	1	0	0

Table S6. Correlations between normalized AUC values and average node activities. Normalized AUC value is a representative value of time-series phosphoprotein array data (see Methods for details). Average node activity is the average value of node states (0 or 1) of 5000 Boolean network models after the models reached their respective attractors under each of conditions. Pearson's correlation coefficient for three condition pairs of normalized AUC and average node activity for each of the antibodies is shown.

Gene symbol	Antibody	Normalized AUC value			Corresponding node	Average node activity			Pearson's correlation coefficient
		Q	S	P		Q	S	P	
PRKAA1	AMPK1/AMPK2 (Ab-485/491)	0.15	0.92	-1.07	AMPK	0.95	0.74	0.47	0.67
CHEK1	Chk1 (Phospho-Ser296)	0.53	0.62	-1.15	ATM/ATR	0.89	0.84	0.40	0.99
CHEK2	Chk2 (Phospho-Thr68)	0.77	0.36	-1.13	ATM/ATR	0.89	0.84	0.40	0.99
CDKN1A	p21Cip1 (Phospho-Thr145)	0.01	1.00	-1.00	CDKN1A	0.90	0.61	0.22	0.58
INSR	IR (Phospho-Tyr1361)	-0.78	1.13	-0.35	INSR	0.07	0.73	0.73	0.68
NFKB1	NFkB-p105/p50 (Phospho-Ser932)	-1.01	0.99	0.02	NF-κB	0.00	1.00	0.00	0.86
PDPK1	PDK1 (Phospho-Ser241)	-1.08	0.18	0.90	PDK1	0.00	1.00	1.00	0.93
PTEN	PTEN (Phospho-Ser380/Thr382/Thr383)	0.71	-1.14	0.43	PTEN	0.71	0.35	0.27	0.47
TSC2	Tuberin/TSC2 (Ab-981)	1.13	-0.35	-0.78	TSC2	0.87	0.57	0.50	1.00
MAP2K1	MEK1 (Phospho-Thr291)	1.14	-0.70	-0.44	MAP2K3/MAP2K6	1.00	1.00	0.00	0.38
MAP2K2	MEK2 (Phospho-Thr394)	1.13	-0.38	-0.76	MAP2K3/MAP2K6	1.00	1.00	0.00	0.65

Table S7. Potential senescence-reversing targets from the ensemble model simulation and supporting evidences.

Gene symbol	Organism	Genetic manipulation	Rejuvenation effect	PMID	$S_{[node]}$
PDK1	-	-	-	-	0.48
PIK3CA	Mus musculus	Suppression	preserved cardiac function, enhanced autophagy, prevented lipofuscin accumulation	19822807	0.4194
AKT1	Mus musculus	Genetic reduction	extended lifespan, decreased oxidative stress, reduced mitochondrial DNA content	23935948	0.3206
IRS1	Mus musculus	Knockout	extended lifespan, delayed age-related processes,	17928362	0.2692
IGF1R	Mus musculus	Knockout	extended lifespan, decreased oxidative stress	12483226	0.2062
KRAS	-	-	-	-	0.1822
INSR	Mus musculus	Knockout	extended lifespan, reduced fat mass	12543978	0.0882

Table S8. Transition trajectory from senescence attractor to quiescence attractor by PDK1 inhibition in the 2401 Boolean network models in which PDK1 is the senescence-reversing target (see the Methods section for more details)

Step / Node	Step1	Step2	Step3	Step4	Step5	Step6	Step7	Step8	Step9	Step10
AKT1	0	0	-0.19	-0.77	-1	-1	-1	-1	-1	-1
AMPK	0	0	0	0	0	0	0	0	0	0
ATM/ATR	0	0	0	0	0	0	0.02	0.04	0.04	0.04
CDK2/4/6	0	0	0	0	0	0	-0.02	-0.03	-0.03	-0.03
CDKN1A	0	0	0	0	0.09	0.20	0.25	0.27	0.27	0.27
CDKN2A	0	0	0	0	0	0	0	0	0	0
DNA damage	0	0	0	0	0	0	0	0	0	0
E2F1	0	0	0	0	0	0	0	0	0	0
EIF4EBP1	0	0	0	0	0	0.10	0.49	0.86	0.96	1
FOXO3	0	0	0	0	0.10	0.22	0.26	0.27	0.28	0.29
IGF1	0	0	0	0	0	0	0	0	0	0
IGF1R	0	0	0	0	0	0	0	0	0	0
IKBKB	0	0	-0.10	-0.53	-0.92	-1	-1	-1	-1	-1
IL1B	0	0	0	0	0	0	-0.01	-0.06	-0.46	-1
IL6	0	0	0	0	0	0	-0.01	-0.06	-0.46	-1
INSR	0	0	0	0	0	0	0	0	0	0
IRS1	0	0	0	0	0	0	0	0	0	0
KRAS	0	0	0	0	0	0	0	0	0	0
MAP2K3/MAP2K6	0	0	0	0	0	0	0	0	0	0
MAPK1	0	0	0	0	0	0	-0.01	-0.03	-0.09	-0.17
MAPK14	0	0	0	0	0	0	0	0	0	0
MDM2	0	0	0	0	0	0	0	0	0	0
MTOR	0	0	0	-0.01	-0.33	-0.79	-0.94	-0.98	-1	-1
NAD+	0	0	0	0	0	0	0	0	0	0
NF-κB	0	0	0	0	0	-0.03	-0.31	-0.84	-1	-1
NFKBIE	0	0	0	0	0.21	0.69	1	1	1	1
PDK1	0	-0.59	-1	-1	-1	-1	-1	-1	-1	-1
PIK3CA	0	0	0	0	0	0	0	0	0	0
PPARGC1A	0	0	0	0	0	-0.01	-0.06	-0.11	-0.12	-0.13
PTEN	0	0	0	0	0.10	0.28	0.36	0.36	0.36	0.36
RB1	0	0	0	0	0	0	0	0	0	0
RHEB	0	0	0	0	0	-0.03	-0.08	-0.10	-0.10	-0.10
ROS	0	0	0	0	0	0	0	0	-0.01	-0.02
S6K1	0	0	0	0	0	-0.10	-0.49	-0.86	-0.96	-1
SGK1	0	0	-0.05	-0.21	-0.27	-0.27	-0.27	-0.27	-0.27	-0.27
SIRT1	0	0	0	0	0	0	0	0	0	0
SOD2	0	0	0	0	0	0.01	0.04	0.07	0.07	0.08
TP53	0	0	0	0	0	0	0	0	0	0
TSC2	0	0	0	0	0.11	0.23	0.26	0.26	0.26	0.26
ULK1	0	0	0	0	0	0.10	0.49	0.86	0.96	1
Low nutrition	0	0	0	0	0	0	0	0	0	0

Table S9. Average node activities of input nodes, positive feedback nodes, and output nodes for each simulation condition. Each of the Boolean networks with the positive feedback loop was given senescence input (DNA damage ON, IGF-1 ON, and low nutrition OFF) to induce the network to its senescence attractor. From the senescence attractor, IGF-1 was turned off and the positive feedback loop was either kept intact or disabled. The positive feedback was disabled by removing the inhibitory regulation of PTEN on PDK1.

Node		Simulation condition		
		IGF-1 on (Senescence)	IGF-1 off & feedback intact	IGF-1 off & feedback disabled
Input	DNA damage	1.00	1.00	1.00
	IGF-1	1.00	0.00	0.00
	Low nutrition	0.00	0.00	0.00
Feedback	PDK1	1.00	1.00	0.39
	AKT	1.00	1.00	0.39
	IKBKB	1.00	1.00	0.37
	PTEN	0.00	0.00	0.63
Output	E2F1	0.00	0.00	0.00
	4E-BP1	0.00	0.00	0.38
	IL-6	1.00	1.00	0.37
	IL-8	1.00	1.00	0.37
	S6K1	1.00	1.00	0.62
	ULK1	0.00	0.00	0.27

Table S10. Signal flow strength for each attractor (see the Methods section for more details)

Source node	Target node	Signal flow strength			
		Senescence	Quiescence	Proliferation	Senescence + PDK1 Inhibition
AKT	CDKN1A	-8.85816	8.85816	-8.85816	8.88738
AKT	FOXO3	-8.7279	8.727899	-8.7279	8.677199
AKT	IKBKB	7.412393	-7.41239	7.412393	-7.41116
AKT	MDM2	8.926647	-8.92665	8.926647	-9.06267
AKT	mTOR	9.169929	-9.16993	9.169929	-10.2393
AKT	PTEN	-8.24408	8.244079	-8.24408	8.191513
AKT	TSC2	-8.62246	8.622461	-8.62246	8.627773
AMPK	FOXO3	-2.49898	8.268279	-4.76761	4.22821
AMPK	mTOR	2.934835	-9.71037	5.599141	-4.49422
AMPK	NAD	-2.50862	8.300169	-4.786	4.212768
AMPK	PPARGC1A	-2.4988	8.267672	-4.76726	4.206369
AMPK	TP53	-2.47324	8.183096	-4.71849	4.033958
AMPK	TSC2	-2.48844	8.233407	-4.7475	4.186648
AMPK	ULK1	-2.79548	9.249304	-5.33328	4.293767
ATM/ATR	TP53	5.699782	6.967192	-1.78363	6.685988
CDK4	RB1	7.686444	8.249182	-1.95205	8.318438
CDKN1A	CDK4	-1.7329	-6.9351	5.003052	-6.79736
CDKN2A	CDK4	-9.04036	-8.97889	9.04036	-9.04018
CDKN2A	MDM2	-12.6043	-12.5186	12.60427	-12.5051
DNA damage	ATM/ATR	8.790273	8.790273	-8.79027	8.795818
DNA damage	MAP2K3/MAP2K6	10.1429	10.1429	-10.1429	10.19209
DNA damage	ROS	9.087676	9.087676	-9.08768	9.09129
FOXO3	ATM/ATR	-2.55056	5.225872	-7.4888	3.83694
FOXO3	CDKN1A	-2.56957	5.264828	-7.54462	3.870794
FOXO3	SOD2	-2.57358	5.273048	-7.5564	3.898509
IGF-1	IGF1R	11.35549	-11.3555	11.35549	11.29168
IGF1R	IRS1	10.86436	-10.8644	10.86436	10.81207
IGF1R	KRAS	9.021828	-9.02183	9.021828	9.074819
IKBKB	IRS1	-6.49986	6.499863	6.499863	6.388083
IKBKB	NFKBIE	-11.0913	11.09129	11.09129	11.08846
IKBKB	PTEN	-8.49735	8.497353	8.497353	8.377729
INSR	IRS1	4.186011	-8.23548	4.186011	4.466589
INSR	KRAS	3.74234	-7.36261	3.74234	4.062817
IRS1	PIK3CA	9.575458	-9.57546	9.575458	9.543578
KRAS	MAPK1	6.725098	-2.52709	6.725098	6.883251
KRAS	PIK3CA	6.68477	-2.51194	6.68477	6.923768
Low nutrition	AMPK	-9.88968	9.88968	-9.88968	-8.79175
Low nutrition	INSR	9.970217	-9.97022	9.970217	9.934797
MAP2K3/MAP2K6	MAPK14	10.94359	10.86917	-10.9436	10.85126
MAPK1	FOXO3	-7.15862	-1.74711	-4.11942	-4.16587
MAPK14	CDKN2A	11.03871	10.96364	-11.0387	11.03953
MAPK14	FOXO3	8.804164	8.744296	-8.80416	8.778331
MAPK14	TP53	9.548533	9.483603	-9.54853	9.600048
MDM2	FOXO3	8.776131	8.776131	-8.77613	8.722368
MDM2	RB1	9.605402	9.605402	-9.6054	9.666615
MDM2	TP53	9.244761	9.244761	-9.24476	9.318338
mTOR	4E-BP1	-9.94088	9.940882	-9.94088	9.933993
mTOR	PPARGC1A	8.591735	-8.59173	8.591735	-8.60965
mTOR	S6K1	9.650598	-9.6506	9.650598	-9.52228
mTOR	ULK1	-9.71722	9.717216	-9.71722	10.34199
NAD	SIRT1	0.991916	4.231252	0.457808	2.960464
NF-κB	IL-8	11.46127	-11.4613	-11.4613	-11.5108
NF-κB	IL-6	11.35748	-11.3575	-11.3575	-11.3789
NF-κB	MAPK1	8.597407	-8.59741	-8.59741	-8.56596
NFKBIE	NF-κB	10.20835	-10.2084	-10.2084	-10.1574
PDK1	AKT	10.63599	-10.636	10.63599	-10.6226
PDK1	IKBKB	8.219922	-8.21992	8.219922	-8.30452
PDK1	SGK1	8.682422	-8.68242	8.682422	-8.73291

PIK3CA	PDK1	11.21337	-11.0922	11.21337	11.34765
PTEN	PDK1	2.712023	-3.56157	3.72168	-3.45902
RB1	E2F1	-10.2671	-10.2671	10.26714	-10.1665
RHEB	mTOR	-2.42029	-4.80313	-2.25349	-4.6378
ROS	MAP2K3/MAP2K6	2.01148	1.555544	-4.46213	1.571911
SGK1	FOXO3	-4.47882	0.041122	-4.47882	0.127836
SIRT1	FOXO3	1.325072	2.450522	1.280329	2.024272
SIRT1	NF-κB	-1.17371	-2.17061	-1.13408	-1.79326
SIRT1	PPARGC1A	1.343995	2.485518	1.298613	2.075555
SIRT1	TP53	-1.32104	-2.44306	-1.27643	-2.0642
SIRT1	TSC2	1.344805	2.487016	1.299396	2.071134
SOD2	ROS	-1.87893	-3.81063	-0.77057	-3.53659
TP53	CDKN1A	8.843193	8.843193	-8.84319	8.772799
TP53	IGF1R	-8.08894	-8.08894	8.088937	-8.10991
TP53	MDM2	4.782981	4.782981	-4.78298	4.713162
TP53	PTEN	8.837121	8.837121	-8.83712	8.88597
TSC2	RHEB	0.678449	-6.70911	1.285104	-5.97605
E2F1	IKBKB	10.54144	10.54144	-10.5414	10.65375
TP53	AMPK	7.283479	7.283479	-7.28348	8.500481

Dataset S1 (separate file). Phosphoprotein array data. Mean fold change between control and treated sample was calculated from quantile normalized values of four samples. Raw intensities of four replicates were also provided.

Dataset S2 (separate file). GO enrichment analysis of phosphoprotein array. For each condition and each time point, we selected genes with log2-transformed quantile normalized raw intensities greater than 13 for GO enrichment analysis. We used EnrichR (4) to perform gene ontology (GO)-term analysis. Adjusted p-value cut-off is 0.001.

SI References

1. V. Pant *et al.*, The p53–Mdm2 feedback loop protects against DNA damage by inhibiting p53 activity but is dispensable for p53 stability, development, and longevity. *Genes & development* **27**, 1857-1867 (2013).
2. X. Wu, J. H. Bayle, D. Olson, A. J. Levine, The p53-mdm-2 autoregulatory feedback loop. *Genes & development* **7**, 1126-1132 (1993).
3. Z.-W. Li *et al.*, The IKKβ subunit of IκB kinase (IKK) is essential for nuclear factor κB activation and prevention of apoptosis. *The Journal of experimental medicine* **189**, 1839-1845 (1999).
4. E. Y. Chen *et al.*, Enrichr: interactive and collaborative HTML5 gene list enrichment analysis tool. *BMC bioinformatics* **14**, 128 (2013).